

Article

Delamination Detection Framework for the Imbalanced Dataset in Laminated Composite Using Wasserstein Generative Adversarial Network-Based Data Augmentation

Sungjun Kim ¹ , Muhammad Muzammil Azad ² , Jinwoo Song ^{2,*} and Heungsoo Kim ^{2,*} 

¹ Smart Materials and Design Laboratory (SMD LAB), Department of Mechanical Engineering, Dongguk University-Seoul, 30 Pildong-ro 1-gil, Jung-gu, Seoul 04620, Republic of Korea; sjkim_400@dgu.ac.kr

² Department of Mechanical, Robotics, and Energy Engineering, Dongguk University-Seoul, 30 Pildong-ro 1-gil, Jung-gu, Seoul 04620, Republic of Korea; muzammilazad@dgu.ac.kr

* Correspondence: jwsong0620@dgu.edu (J.S.); heungsoo@dgu.edu (H.K.); Tel.: +82-2-2260-8577 (H.K.); Fax: +82-2-2263-9379 (H.K.)

Abstract: As laminated composites are applied more commonly, Prognostics and Health Management (PHM) techniques for the maintenance of composite systems are also attracting attention. However, applying PHM techniques to a composite system is challenging due to the data imbalance problem from the lack of failure data and unpredictable failure cases. Despite numerous studies conducted to address this limitation, including techniques like data augmentation and transfer learning, significant challenges remain. In this study, the Wasserstein Generative Adversarial Network (WGAN) model using a time-series data augmentation technique is proposed as a solution to the data imbalance problem. To ensure the performance of the WGAN model, time-series data augmentation of experimental data is executed with a frequency analysis. After that, a One-Dimensional Convolutional Neural Network (1D CNN) is used for fault diagnosis in laminated composites, validating the performance improvement after data augmentation. The proposed data augmentation significantly elevated the performance of the 1D CNN classification model compared to its non-augmented counterpart. Specifically, the accuracy increased from 89.20% to 91.96%. The precision improved remarkably from 29.76% to 74.10%, and its sensitivity rose from 33.33% to 94.39%. Collectively, these enhancements highlight the vital role of data augmentation in improving fault diagnosis performance.

Keywords: PHM; fault diagnosis; data imbalance; laminated composite; WGAN



Citation: Kim, S.; Azad, M.M.; Song, J.; Kim, H. Delamination Detection Framework for the Imbalanced Dataset in Laminated Composite Using Wasserstein Generative Adversarial Network-Based Data Augmentation. *Appl. Sci.* **2023**, *13*, 11837. <https://doi.org/10.3390/app132111837>

Academic Editors: Roque A. Osornio-Rios, Athanasios Karlis and Andres Bustillo Iglesias

Received: 27 September 2023

Revised: 20 October 2023

Accepted: 27 October 2023

Published: 29 October 2023



Copyright: © 2023 by the authors. Licensee MDPI, Basel, Switzerland. This article is an open access article distributed under the terms and conditions of the Creative Commons Attribution (CC BY) license (<https://creativecommons.org/licenses/by/4.0/>).

1. Introduction

With their high specific strength, stiffness, and resistance to both corrosion and heat, composite structures are increasingly replacing metallic structures in various engineering applications, including aerospace, marine, automobile, and infrastructure [1,2]. Composite structure has orthotropic, layered structure and complexity in the manufacturing process. Due to these natural characteristics, various fault modes, such as matrix crack, fiber breakage, and delamination, often occur, and this makes it difficult to apply composite structures in the actual industrial field [3,4]. Among these various failure modes, delamination or inter-ply separation is the most critical defect. These types of failure exist in the inner surface and are not observable without technical equipment, leading to sudden fracture of the structure and a huge loss of various resources [5,6]. To avoid structural failure and severe loss, it is necessary to quickly detect damage in composite structures to prolong their service life. PHM technology provides early damage detection and helps avoid the deterioration of various industrial systems [7–12]. Recently, techniques for PHM based on Machine Learning (ML) and Deep Learning (DL) using vibration signals have been continuously adopted for fault diagnosis in various structures. They have the ability to detect

unseen defects in the interior of the structure, and using the vibration data demonstrates high fault diagnosis performance [13–16].

Initially, conventional Machine Learning (ML) model-based fault diagnosis was mainly used, in which engineers manually extracted features related to the faults of the system and diagnosed the condition of the system [17]. Features extracted from signals are generally from the time domain, frequency domain, and time–frequency domain [18]. Time domain features vary from conventional values, for example, the mean, standard deviation, peak, amplitude square, and Root Mean Square (RMS), to combinations of these features, like the waveform factor, peak factor, margin factor, and central moment [19,20]. For more detailed information, frequency, as well as time–frequency domain features, could also be derived from the Fourier transform, short-time Fourier transform, wavelet transform, and wavelet packet transform [21–23]. Because features related to frequency analysis contain the dynamic behavior of the system, they can offer more sensitive and thorough information about the system. The extracted features are then utilized to predict whether the system is in a normal or fault state. ML models, such as K-Nearest Neighbor (KNN), Support Vector Machine (SVM), and Decision Tree, are trained by part of the extracted features, while the rest of the features are exploited to test whether the trained model can properly decide the health state of the system [24–26].

Although fault diagnosis using ML showed remarkable performance, it was time consuming, and a massive theoretical background was needed to extract features manually from the data. To overcome this limitation, Deep Learning (DL) techniques started to be utilized for fault diagnosis. The DL model can extract features automatically by using its neural network and classify the health state of the system. The Convolutional Neural Network (CNN) model is generally used for fault diagnosis owing to its outstanding feature extraction performance from motor current signals, vibration signals, and multi-variate signals [27–30]. Raw signals are converted into images that can represent the health state of the system, like spectrogram, scalogram, or various sorts of grey-scale images. The CNN model extracts features from these images and then predicts whether the system is in a normal state. The Vision Transformer (ViT) model is also utilized for fault diagnosis using image data [31]. The ViT model can extract features from the local part of an image and classify the health state of the system. Transfer learning models that are pretrained on a large amount of image datasets are widely applied for fault diagnosis. Among the various models, Residual Network-50 (Resnet-50) is generally used [32]. Long Short-Term Memory (LSTM) and Bidirectional LSTM (BiLSTM) are other deep learning-based methods for fault diagnosis. They have a unique ability to extract features from time series data; they have remarkable performance in predicting Remaining Useful Life (RUL), as well as fault diagnosis. The models use extracted features from the raw time-series signal itself or preprocessed signals to perform fault diagnosis [33–36].

Although DL-based fault diagnosis has been explored by many researchers, numerous limitations still remain. For general applications of fault diagnosis using DL models, further research is required to address challenges, such as noise mitigation, data imbalance, and various uncertainties. In particular, data imbalance, where certain classes in the dataset have fewer instances, can significantly reduce the performance of the DL model. The model may struggle to learn features of the minority class, resulting in lower accuracy for that class [37]. In addition, since there is a myriad of unpredictable damage cases with a diverse range of operating and environmental conditions, it is impractical to comprehensively detect and anticipate all potential damages in advance. To cope with these challenges, it is essential to generate synthetic data through experimentation, simulation, or data-driven approaches. However, the process of data acquisition through experiments or simulations can be both time-consuming and financially burdensome. Additionally, these methods require an in-depth understanding of the physics of the composite structure [38]. To address these challenges, a focus has been placed on developing data-driven approaches to generate synthetic data. These methods require less in-depth understanding of the physics involved and are less labor-intensive by leveraging advanced algorithms and DL techniques.

Above all, there are some basic data augmentation techniques that use simple mathematical calculations. For example, images from impact response data can be manipulated by adding and multiplying by random numbers [39]. Similarly, adding Gaussian noise to the images obtained from acoustic emission and guided wave signals was also performed [40,41]. The advantage of this type of data augmentation method is the low level of difficulty. They are easy to implement, and the corresponding algorithms are not complex. Other simple methods—such as shifting, scaling, rotating, and random grid shuffling of the images—are also performed [42]. These are also basic techniques for data augmentation for images. However, in most engineering problems, images contain some dynamic characteristics of the system, including time, amplitude, and frequency of the signal. Therefore, this kind of augmentation technique should be applied with caution regarding the engineering problem. Recently, data augmentation using the GAN model for image data has been widely used [43–45]. By using the GAN model, it is possible to duplicate the dynamic characteristics of the original data and thus generate synthetic image data properly.

Although these approaches can generate sufficient data for robust fault diagnosis in composite structures, most of them rely on image-based data augmentation. Thus, this approach necessitates proper preprocessing of raw data for their transformation into 2D images, making the process tedious and time-consuming. Therefore, data augmentation of the raw time-series signal, not imagery, can benefit by eliminating the need for excessive preprocessing, making the PHM process for composite structures simple and computationally efficient.

To tackle the issues mentioned above, this paper proposes a time-series data augmentation technique using the Wasserstein Generative Adversarial Network (WGAN) model. WGAN is a type of DL model that can accurately capture the distribution of the training data. Thus, it can generate synthetic data that maintain identical dynamic characteristics with the training data. For this reason, an in-depth understanding of the physics of the composite structures is less necessary to use the WGAN model to generate the synthetic data. As a tool to validate the proposed data augmentation method, fault diagnosis in laminated composite structure using the One-Dimensional Convolutional Neural Network (1D CNN) model was implemented. The 1D CNN can extract features directly from time-series signals, and no preprocessing is needed for the use of input data. Therefore, the total time for both preprocessing and training is reduced.

To validate the proposed data augmentation methodology, an initial experiment was conducted to obtain vibration data from composite specimens. Three different health states of composite specimens—healthy, delamination 1, and delamination 2—were manufactured. Vibration signals from these states were then captured using a shaker and computer software. The amount of data collected for the healthy state was intentionally made much larger than the damaged ones to simulate the data imbalance problem. Then, data augmentation was performed across all health states. After data augmentation, a fault diagnosis was conducted using the 1D CNN model on two different datasets: a dataset consisting of only experimental data and a dataset composed of synthetic data. Then, the two results were compared to assess the data augmentation capabilities of the WGAN model. Afterward, a comparative analysis was performed to highlight the superior data augmentation ability of the WGAN model by comparing it with various oversampling and other data augmentation methods.

The rest of this paper is composed as follows: Section 2 presents the background of previous methods for data augmentation and the fault diagnosis model for this research. Section 3 illustrates the experimental setup to validate the suggested methodology. Section 4 describes the fault diagnosis results and provides a comparative analysis. Finally, Section 5 concludes this research, outlining its contributions and suggesting directions for future research.

2. Proposed Methodology

2.1. Overview

In this section, solutions for the data imbalance problem and fault diagnosis methodology are proposed. Section 2.2 briefly introduces the theoretical background of previous methods for oversampling and data augmentation, which is later utilized in Section 4. Then, Section 2.3 describes the mathematical formula of the WGAN model for time-series vibration data augmentation. Finally, Section 2.4 explains the fundamental contents of the 1D CNN model for fault diagnosis.

2.2. Previous Works

2.2.1. Adaptive Synthetic Sampling

Although several techniques have been developed to address data imbalance, methods that directly augment the minority class by generating synthetic data have gained significant attention. Adaptive Synthetic Sampling (ADASYN) is an oversampling technique based on the K-Nearest Neighbor (KNN) algorithm, considering the distribution of the minority and majority classes. ADASYN generates synthetic data by interpolating between existing data points within the minority class rather than merely duplicating the original data [46]. In the minority class, the basis data point is decided as a fixed point to apply the KNN algorithm, and the nearest neighbor value is selected. After the nearest neighbors are chosen, the linear interpolation method of Equation (1) is used to generate synthetic data between the basis data point and the nearest neighbors, where α is a random value from 0 to 1.

$$s_j = (1 - \alpha) \times p_i + p_{ij}, i, j = 1, 2, 3 \dots \quad (1)$$

Here, data points in the majority class, which exist in the inner area of the nearest neighbor boundary, are considered. The ratio of data points within the majority class is calculated according to Equation (2), where δ_i is the number of data points in the majority class in the nearest neighbor boundary for the i -th nearest neighbor, and K is the total number of nearest neighbors.

$$r_i = \frac{\delta_i}{K}, i = 1, 2, 3 \dots \quad (2)$$

ADASYN generates more synthetic data if r_i is larger than the others. Owing to this comparison process of data distribution, synthetic data could be distributed to maintain distinct characteristics compared to the data from other classes.

2.2.2. System Identification

While ADASYN focuses on generating synthetic data for the minority class based on the distribution of classes and neighboring data points, another approach to tackle data imbalance is through System Identification (SI). The SI process builds a mathematical dynamic model of the system by using the measured input and output signals. The SI technique is an important part of modern control theory [47] and has been used as a data augmentation to overcome data imbalance and the data scarcity problem [48]. The input and output signals of the system are used to reconstruct the discrete system matrix A_r , B_r , C_r , D_r , which is expressed as a state space model, where A_r is the realized system matrix, B_r is the realized input matrix, C_r is the realized output matrix, and D_r is the transmission matrix [49]. After these matrices are defined, unseen signals are used as input for the realized matrices. As a result, synthetic signals, which are augmented signals, could be obtained. The SI technique can restore the system dynamics by using only single input and output signals, which means that it does not need multiple pairs of signals. Because of this advantage, it could be used as a great solution for data imbalance and the scarcity problem, as mentioned above.

2.2.3. Generative Adversarial Network

The GAN model, originally proposed to produce real-like images from Gaussian noise input, has also been developed to generate synthetic time-series data [50–53]. The GAN model is composed of two deep learning models: generator and discriminator. The generator generates synthetic data by using Gaussian noise input. The discriminator gets real data and synthetic data as input data and discriminates whether the input data are real or synthetic. By using the training results of these models, parameters are updated to produce realistic synthetic data, which means that the synthetic data distribution p_z has a similar distribution to the real data $p_{data(x)}$. The loss function of the GAN model is written as Equation (3), which is the deformed shape of the Jensen–Shannon Divergence (JSD), where $D(x)$ is the discriminator output, and $G(z)$ is the generator output.

$$\max_{\min} V(D, G) = E_{x \sim p_{data(x)}} [\log D(x)] + E_{z \sim p_z(z)} [\log(1 - D(G(z)))] \quad (3)$$

The generator and discriminator keep training to deceive each other until the models reach the Nash Equilibrium. Figure 1 illustrates the training process of the general GAN model.

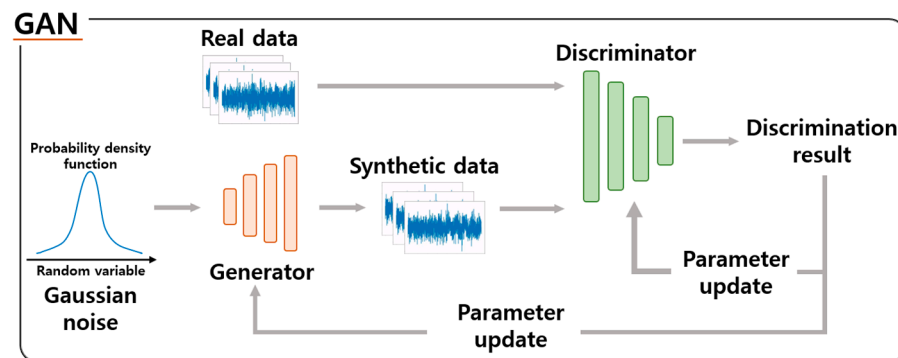


Figure 1. Training process of the GAN model.

Although the GAN model shows remarkable data augmentation performance, its mathematical nature raises several critical points. There are two main limitations to the application of the GAN model: gradient vanishing and mode collapse [54,55]. Both problems arise from the loss function of the GAN model. The fundamental concept of the GAN model is a minimax game in which the discriminator tries to maximize the loss function while the generator attempts to minimize the loss function. In this process, if the discriminator is trained better than the generator, the gradient of the generator becomes 0 according to Equation (3), and the generator cannot be trained properly. This is called gradient vanishing. Also, when the generator generates synthetic data in multiple classes, the generator only tries to deceive the discriminator and does not consider the information about each class. As a result of this characteristic, the training process of the generator could be biased to specific weights, which means the generator only generates data belonging to a specific class, not evenly. Simply, the generator falls into a local minimum problem and cannot imitate the distribution in any other classes except one class. This is called mode collapse.

Due to the drawbacks mentioned above, instability in training the GAN model often takes place. This makes it hard to converge the generator and discriminator, reducing the performance of the GAN model. Numerous unrevealed factors may exist in this instability, but one of the fundamental reasons is the loss function. The loss function that uses JSD could output 0 or too large a number, as mentioned above, leading to the submission of meaningless gradients to the generator and discriminator. To overcome these vulnerabilities, various GAN models that use different loss functions have been introduced.

2.3. Wasserstein Generative Adversarial Network

As outlined in Section 2.2.3, the limitations for GAN arise from the generator receiving meaningless gradients. To provide the generator with meaningful gradients, employing an alternative loss function is essential. WGAN uses Earth Mover's Distance (EMD) or Wasserstein distance as loss functions, which can be expressed as Equation (4).

$$W(\mathbb{P}_r, \mathbb{P}_g) = \inf_{\gamma \in \Pi(\mathbb{P}_r, \mathbb{P}_g)} \mathbb{E}_{(x,y) \sim \gamma} [\|x - y\|] \quad (4)$$

Here, $\Pi(\mathbb{P}_r, \mathbb{P}_g)$ represents all sets of the joint distributions $\gamma(x, y)$, which have $\mathbb{P}_r, \mathbb{P}_g$ as marginal individually. The intuitive definition of the Wasserstein distance means the quantity of mass that must be transported from x to y for the distribution of the generated data \mathbb{P}_g to align with the distribution of real data \mathbb{P}_r .

However, it is impossible to apply the Wasserstein distance in Equation (4) directly as a loss function because it is almost impossible to find all the joint distributions and minimum values. Due to this restriction, Kantorovich–Rubinstein duality is introduced, which constrains the objective function by using the 1–Lipshitz method [56]. In this context, since it is difficult to identify the exact function we want to constrain, the objective function is approximated using a neural network. After applying the Kantorovich–Rubinstein duality and 1–Lipshitz method, the loss function using Wasserstein distance turns into Equation (5).

$$\text{Loss function} = \max_{w \in W} \mathbb{E}_{x \sim \mathbb{P}_r} [f_w(x)] - \mathbb{E}_{z \sim p(z)} [f_w(g_\theta(z))] \quad (5)$$

Here, f_w denotes a function approximated by the neural network that has variables of w , and similarly, g_θ is a function that involves variables of θ . For brevity of the study, detailed mathematical formulae of the Kantorovich–Rubinstein duality and Lipshitz method are omitted.

The gradients for updating WGAN must be restricted because it does not use the sigmoid function for the last layer of the discriminator. This could potentially lead to unbounded output values and destabilizing gradients during the training process. For this purpose, the ‘weight clipping’ technique is used to restrict the scale of the gradients between -0.01 and 0.01 . Because of this mathematical difference between the discriminator in the conventional GAN and the discriminator in WGAN, the latter one is named the ‘critic’. Through this overall process in WGAN, the generator can obtain proper gradients, and the training generator and critic can be balanced. Furthermore, through generating meaningful gradients, the stability of the training process can be improved.

2.4. One-Dimensional Convolutional Neural Network

Over recent years, there has been significant research interest in the Two-Dimensional Convolutional Neural Network (2D CNN) model-based fault diagnosis because it has a remarkable ability to automatically extract features from the images [57,58]. However, 2D CNN requires various data preprocessing techniques, especially when used with vibration signals. For this application, the signal has to be converted into spectral images, making the fault diagnosis procedure more complex and laborious. Also, 2D CNN takes a longer time for training and testing, which may not be suitable for real-time fault diagnosis. For these reasons, this research employs the One-Dimensional Convolutional Neural Network (1D CNN), using time-series vibration signals directly as input for fault diagnosis.

The 1D CNN can directly extract features from time-series signals without data preprocessing. Contrary to 2D CNN, convolution and pooling size can extract one-dimensional features from a time-series signal. Also, the training speed of the 1D CNN is much quicker than that of the 2D CNN because the input data size for the 1D CNN is smaller, and 1D CNN does not need additional preprocessing techniques since time-series data are directly used as input. This makes the 1D CNN more resource-efficient, leading to cost savings without decreasing the fault diagnosis performance. Owing to these advantages,

1D CNN is continuously applied for fault diagnosis in various systems [59,60]. Details of the structures of the 1D CNN used in this research are later discussed in Section 4.2.

3. Experimental Validation

Section 3 describes the experimental validation process to ensure the performance of the suggested data augmentation and fault diagnosis techniques. Section 3.1 explains the experimental setup to obtain the imbalanced vibration dataset, while Section 3.2 describes the data augmentation process using the WGAN model to resolve the data imbalance problem and the validation of the synthetic data involved.

3.1. Experimental Setup and Data Acquisition

Laminated composite plates are manufactured to obtain an imbalanced vibration dataset. Eight layers of carbon prepreg (T700SC-12k-60E), which have dimensions of 35 cm × 30 cm, are stacked in $[0/90/0/90]_s$ order, as shown in Figure 2. Table 1 shows the mechanical properties of the prepreg.

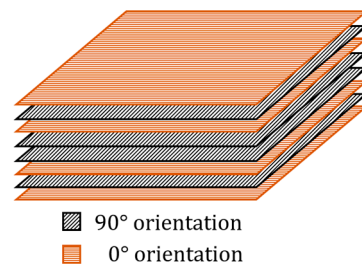


Figure 2. Laminated angles for each layer in the composite structure.

Table 1. Mechanical properties of the carbon prepreg.

Tensile Modulus	Tensile Strength	Elongation	Thermal Conductivity	Density	Filament Diameter
230 GPa	4900 MPa	2.1%	9.4 W/m·K	1.8 g/cm ³	7 µm

To imitate various health states of the laminated composites, Teflon film (Model KSC-V1000) with a thickness of 0.03 mm and a usable heating range of 280 °C was inserted between the fourth and fifth layers during the stacking. The film can act like damage inside the laminated composite, so the presence of delamination could be imitated. A total of three health states of composite plates are stacked: Healthy (H), which has no delamination, and Delamination 1 (D1) and Delamination 2 (D2), which have delamination in different locations inside of the specimens.

After stacking, the plates were cured using the hot press machine illustrated in Figure 3a. The pressure of the machine was 20 kg/cm², and the heating cycle of the plate is in Figure 3b. The cured plates that have dimensions of 35 cm × 30 cm are then cut into five pieces to receive a beam-shape of 35 cm × 5 cm, as shown in Figure 4. Thus, five specimens for each health state, and a total of fifteen specimens, were manufactured for all health states. The blue-colored area is used as the fixed part for the vibration experiment, while the red-colored area indicates the presence of delamination.

Figure 5 shows the Data Acquisition system. Random vibration signals were generated through MATLAB Simulink, and they were collected in the Data Acquisition (DAQ) unit (DAQ1, model dSPACE/CLP1104). The magnitude of signals was enlarged through the amplifier (model Labworks/PA-151). These amplified signals were then received by a shaker (model Labworks/ET-126-4), which induced vibration in the specimen.

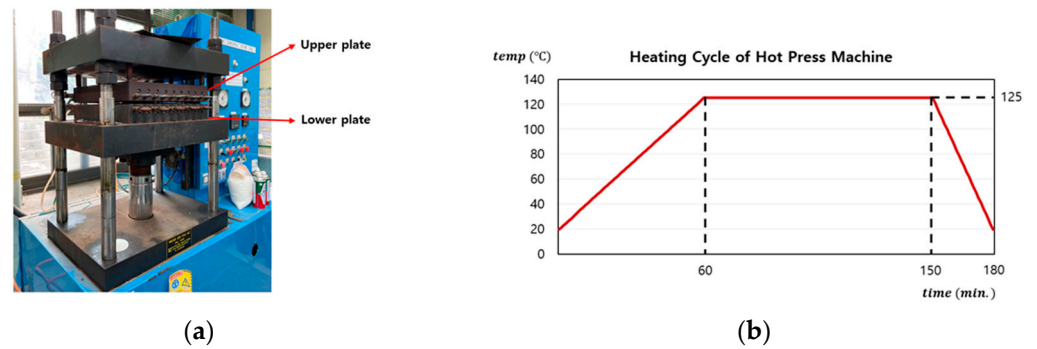


Figure 3. (a) Hot press machine used for manufacturing specimen. (b) Heating cycle for the hot press machine.

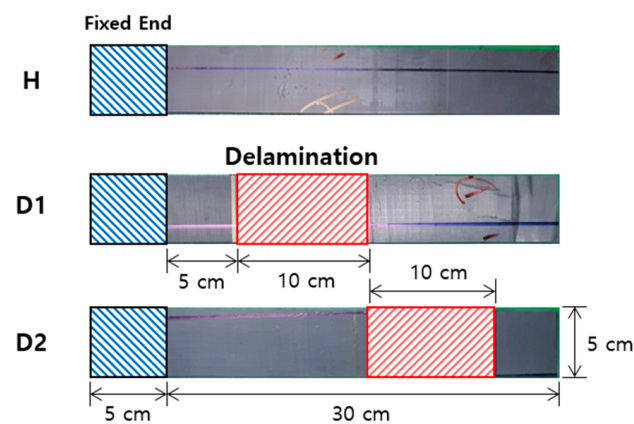


Figure 4. Three health states of the manufactured specimens.

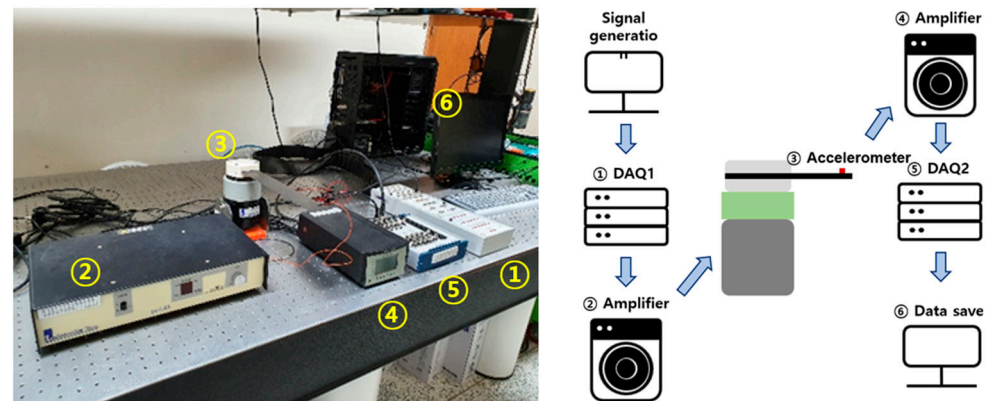


Figure 5. Data acquisition system for the experiment.

Response signals were obtained with accelerometer (model Bruel & Kjaer/Type 4517-C) sensors that were bonded on the top surface of the specimens. Herein, for the robustness of variations in signals, signals were acquired through the same ten sensors but in different locations. Figure 6 shows the locations of the accelerometers. The figure shows that the sensors were bonded near the edges to consider the effects of twisting and bending in the specimen.

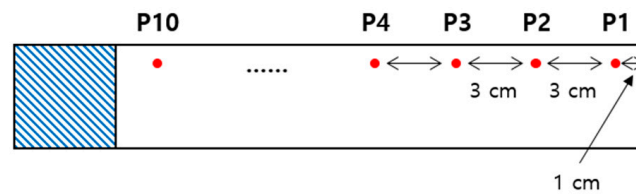


Figure 6. The ten different accelerometer locations for the research.

The response signals from the sensors were then put into the amplifier (model Bruel & Kjaer/Type 2692-0s2) again, and after passing the DAQ (DAQ2, model NI/USB-6341), the final response vibration signals were saved in the computer.

To simulate the imbalance problem in the experimental condition, a different number of sensors were selected for each health state. For state H, sensors from P1 to P10 were used, while for states D1 and D2, only P01 was used. For state H, 1000 signals were obtained for each sensor, and 60 signals for D1 and D2 were acquired to maximize the data imbalance problem. Because five specimens for each health state were utilized to obtain the dataset, 200 data instances for H and 12 data instances for D1 and D2 each were acquired from each specimen. Table 2 shows the number of the dataset and length of the signals for each health state.

Table 2. Description of dataset for each health state.

	Healthy	Delamination 1	Delamination 2
Number of sensors	P01–P10	P01	P01
Number of data	1000	60	60
Signal length	1875	1875	1875

3.2. Data Augmentation Using WGAN Model

To validate the proposed method, data augmentation was performed using the WGAN model illustrated in Figure 7. The structure of the WGAN model and model parameters listed in Table 3 are determined through a process of trial and error because there is no specific standard or technique.

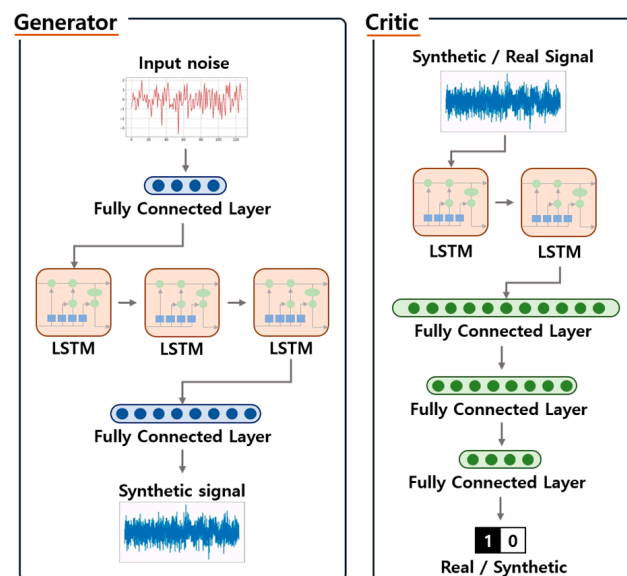


Figure 7. Structures of the generator and critic for the research.

Table 3. Model parameters of the WGAN model for each health state.

	Healthy	Delamination 1	Delamination 2
Beta 1	0.5	0.5	0.5
Beta 2	0.9	0.9	0.9
Training critic/Training generator	3	5	5
Learning rate	3×10^{-4}	3×10^{-4}	3×10^{-4}
Epoch	2000	2000	2000
Batch size	8	8	8

For the Healthy state, since it takes a significant period to generate synthetic signals for all pairs, signals from sensors in the same location have similar dynamic characteristics. Thus, synthetic signals were generated by only considering sensor location. With data augmentation, with 300 signals per sensor, a total of 3000 signals were generated. For Delamination 1 state, three specimens, D1-1, D1-2, and D1-3, were utilized individually to obtain 1000 synthetic signals per specimen. Similarly, Delamination 2 state used three specimens and acquired 1000 signals per specimen. For delamination cases, delamination in the specimens was manufactured by manually inserting the Teflon films. Therefore, there are slight differences in dynamic characteristics for different specimens. In this perspective, data augmentation for delamination cases was conducted for each specimen. There were 1000 synthetic signals for each specimen; a total of 3000 signals were generated.

4. Fault Diagnosis Results

4.1. Evaluation Metrics

Evaluation metrics are employed to evaluate the classification performance of a DL model. These metrics are calculated by using the predicted labels from the DL model and comparing them with the actual labels. Figure 8 shows the relationships and denotations of these metrics, while Equations (6)–(9) provide the formulae for these evaluation metrics. Accuracy is an intuitive metric with which to evaluate the classification performance; it quantifies the proportion of predicted labels that match the actual labels, including both true and false predictions. Precision is the ratio of actual true labels to the labels that the model predicted as true. Sensitivity is the ratio of the labels that the model predicted as true to the actual true labels. The F1 score is the harmonic average of the precision and sensitivity. All metrics reinforce the weakness of others and thus can evaluate the classification performance of the model.

$$\text{Accuracy} = \frac{\text{TP} + \text{TN}}{\text{TP} + \text{FN} + \text{FP} + \text{TN}} \quad (6)$$

$$\text{Precision} = \frac{\text{TP}}{\text{TP} + \text{FP}} \quad (7)$$

$$\text{Sensitivity} = \frac{\text{TP}}{\text{TP} + \text{FN}} \quad (8)$$

$$\text{F1 score} = 2 \times \frac{\text{Precision} \times \text{Sensitivity}}{\text{Precision} + \text{Sensitivity}} \quad (9)$$

		Actual label	
		True	False
Predicted label	True	True Positive (TP)	False Positive (FP)
	False	False Negative (FN)	True Negative (TN)

Figure 8. Denotations of the predicted and actual labels.

4.2. Fault Diagnosis Results

In this section, fault diagnosis was performed on the experimental data and synthetic data to evaluate the effectiveness of data augmentation. Figure 9 shows the 1D CNN model structure that was used for fault diagnosis, and Table 4 indicates the detailed information of the model. To maintain the uniformity of the research, the same 1D CNN model structure was applied in all instances of fault diagnosis. Considering complex embedded information in the random signal, the model is constructed with several Convolutional–Maxpooling pairs. To activate the nonlinearities from convolution layers, the ReLU activation function was applied. After extracting features, the dropout layer was added after the dense layer to reduce overfitting due to its complex model structure.

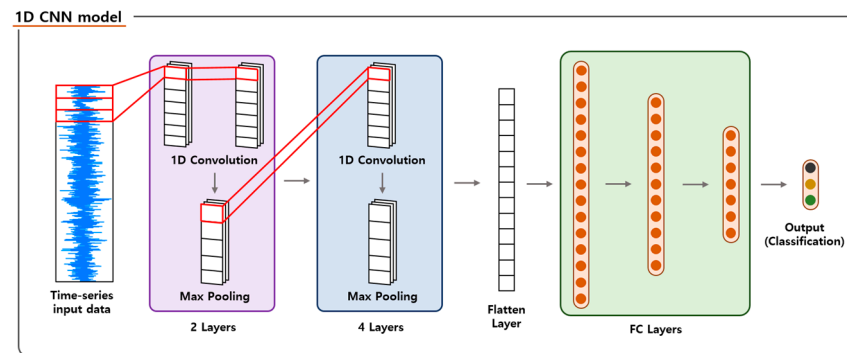


Figure 9. Structure of the 1D CNN model for the research.

Table 4. Detailed information of 1D CNN model for the research.

Network Layer	Output Data Size	Parameters
Input Layer	1875×1	1875 length signal input
Conv1D	1875×32	$32 @ 3 \times 1$, stride = 1, activation = ReLU
Conv1D	1875×32	$32 @ 3 \times 1$, stride = 1, activation = ReLU
Max pooling 1D	937×32	2×1 , stride = 2, activation = ReLU
Conv1D	937×64	$64 @ 3 \times 1$, stride = 1, activation = ReLU
Conv1D	937×64	$64 @ 3 \times 1$, stride = 1, activation = ReLU
Max pooling 1D	468×64	2×1 , stride = 2, activation = ReLU
Conv1D	468×128	$128 @ 2 \times 1$, stride = 1, activation = ReLU
Max pooling 1D	234×128	2×1 , stride = 2, activation = ReLU
Conv1D	234×128	$128 @ 2 \times 1$, stride = 1, activation = ReLU
Max pooling 1D	117×128	2×1 , stride = 2, activation = ReLU
Conv1D	117×256	$256 @ 2 \times 1$, stride = 1, activation = ReLU
Max pooling 1D	58×256	2×1 , stride = 2, activation = ReLU
Conv1D	58×256	$256 @ 2 \times 1$, stride = 1, activation = ReLU
Max pooling 1D	29×256	2×1 , stride = 2, activation = ReLU
Flatten Layer	1×7424	7424 neurons
Input Layer	1×7424	7424 neurons
Dense	1×1024	1024 neurons
Dropout	1×1024	Dropout rate: 0.4
Dense	1×512	512 neurons
Dropout	1×512	Dropout rate: 0.4
Dense	1×128	128 neurons
Dropout	1×128	Dropout rate: 0.4
Dense	1×3	128 neurons
SoftMax	1×3	Classification Layer

For the 1120 signals in the experiment, they were randomly divided into 60%, 20%, and 20% for training, validation, and testing of the model while maintaining the proportion of the data for each class. After generating synthetic signals with the WGAN model, as written in Section 3.2, they were used for training and validation data with the same 1D

CNN model structure. For each health state, 3000 signals were generated, 9000 in total. Then, synthetic signals were randomly divided into a 60% allocation for training data and a 40% allocation for validation data while maintaining the class proportion. To demonstrate the enhanced fault diagnosis performance, the test dataset for the experimental data case was used for both cases. Because the data were divided randomly, test data may contain some identical data used for data augmentation. However, this fault diagnosis result could bring meaningful conclusions for the solution of the data imbalance problem.

The test results are shown in Figure 10. For the experimental data case, because of the severe data imbalance problem, the training process of the 1D CNN model is biased for a healthy state, dropping the fault diagnosis performance of fault states, as shown in Figure 10a. This bias caused the 1D CNN model to diagnose the fault state improperly, showing inferior fault diagnosis performance. The test result for synthetic data is depicted in Figure 10b. Compared to the results from the experimental data, the performance for the healthy state decreased slightly. However, the classification results for faulty states increased dramatically; 23 cases were predicted correctly out of 24 cases. From this, it could be concluded that the proposed data augmentation technique increased the overall fault diagnosis performance.

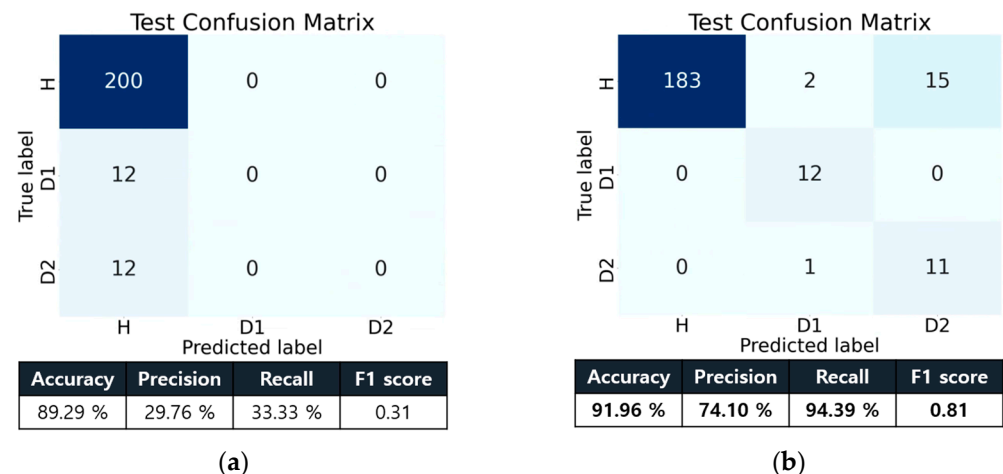


Figure 10. (a) Fault diagnosis results for the experimental data only. (b) Fault diagnosis results for the synthetic data.

At first glance, the accuracy seems to show only a negligible improvement, rising from 89.29% to 91.96%. However, the other metrics, precision and sensitivity, showed much-improved outcomes. The precision surged from 29.76% to 74.10%, while the sensitivity soared from 33.33% to 94.39%. These differences in results across the metrics derive from the imbalanced nature of the dataset. Imbalanced datasets can often lead to misleading accuracy metrics, as the model might perform very well on the majority class but poorly on the minority class. In such cases, precision and sensitivity provide a more accurate understanding of the model's performance, especially in identifying and classifying the underrepresented class.

4.3. Comparative Analysis

To demonstrate that the WGAN model is the best solution for addressing the data imbalance problem in the vibration signal, a comparative analysis was conducted between the WGAN model and the other methods of ADASYN, SI, and GAN. Table 5 describes the model parameters of the GAN model. The same structure of the discriminator and generator as the WGAN model was used and the corresponding parameters were adjusted by trial and error. Through the parameter optimizing results, it was observed that even though the same discriminator and critic models were utilized, the parameters were completely different according to the type of loss function.

Table 5. Model parameters of the GAN model for each health state.

	Healthy	Delamination 1	Delamination 2
Beta 1	0.5	0.5	0.5
Beta 2	0.999	0.999	0.999
Learning rate	1×10^{-3}	1×10^{-3}	1×10^{-3}
Epoch	1200	1200	1200
Batch size	8	8	8

Table 6 shows the number of synthetic data for each method. Basically, the ADASYN algorithm is an oversampling method, which means that it can only generate minority class data, the D1 and D2 cases in this research. Therefore, the total amount of data is different from the other methods. For all the methods, synthetic data instances were randomly divided into 60% and 40% for training and validation while maintaining the proportion of each class.

Table 6. The number of synthetic data for training and validation using the different methods.

	Healthy	Delamination 1	Delamination 2
Experimental data only	800	48	48
ADASYN	800	793	798
SI	3000	3000	3000
GAN	3000	3000	3000
WGAN	3000	3000	3000

Table 7 shows the fault diagnosis results for the same test dataset as Section 4.2. The accuracy of the WGAN model was the highest result at 91.96%. Also, the experimental data-only case has relatively higher accuracy than the other methods. As mentioned above, this originates from the data imbalance. The majority of the class data was classified properly; thus, the accuracy itself turned out to be high. For precision, ADASYN was the highest, at 77.80%, with a difference of 3.70% compared to the WGAN model. For sensitivity, WGAN had the highest value at 94.39%, which is 3.11% higher than the ADASYN. By comparing the precision and sensitivity of the ADASYN and WGAN, WGAN seems to have a better ability to identify fault states properly. The health state data for ADASYN may be classified more properly than that for WGAN, and this point brought higher precision in ADASYN but lower performance in sensitivity. For the F1 score, ADASYN and WGAN were the highest at 0.81.

Table 7. Fault diagnosis result of each oversampling and augmentation method.

	Accuracy (%)	Precision (%)	Sensitivity (%)	F1 Score
Experimental data only	89.29	29.76	33.33	0.31
ADASYN	90.63	77.80	91.28	0.81
SI	5.80	35.13	35.00	0.04
GAN	86.61	53.83	55.83	0.55
WGAN	91.96	74.10	94.39	0.81

For overall analysis, the synthetic data generated with SI seems not to be proper for this research because all evaluation metrics were much lower than the other methods. In the case of ADASYN, because of the characteristic of oversampling, real data are contained in the training and validation datasets, while the rest of them are only composed of synthetic data. This could increase the fault diagnosis performance compared with the others. For the ADASYN, GAN, and WGAN cases, the evaluation metrics increased significantly compared to the experimental data case, but the WGAN model showed the best evaluation metrics, which means that the WGAN model can generate signals that contain dynamic characteristics that are the same as real signals.

5. Conclusions

This study addresses the time-series data augmentation technique using the WGAN model for the solution of the data imbalance problem and fault diagnosis using the 1D CNN model. For time-series data augmentation, vibration signals were directly used as input data for the WGAN model. To verify the performance increase in fault diagnosis by applying the WGAN model, experiments using laminated composite beam specimens to obtain vibration signals were conducted. For imitation of the data imbalance dataset, 1000 signals for the healthy state and 60 signals for faulty states were obtained through the experiments, and a total of 9000 synthetic signals were generated by using the WGAN model. To verify the enhanced fault diagnosis performance, the results from a 1D CNN model using both experimental and synthetic datasets were compared. The results demonstrated a significant improvement in fault diagnosis. Furthermore, a comparative study revealed that data augmentation with the WGAN model yielded the best diagnostic performance.

In contrast to previous works, this research has simplified the data augmentation and fault diagnosis process by directly using time-series data as input. The simplification of the process saves computational resources because both the WGAN and 1D CNN models use time-series data, which has a smaller data size than the image data. Thus, training time, as well as predicting time, are also much shorter, which means the enhanced probability of applications in real-time fault diagnosis. For the last contribution, fault diagnosis could be performed by inexpensive and simple experiments. The accelerometer is a cheap sensor among various sensors, which means that data can be obtained efficiently.

Notwithstanding these contributions to the solution of the data imbalance problem and the fault diagnosis process, some limitations still exist. After the advent of the GAN model, much research related to GAN has been conducted, but a generalization of the GAN model for various engineering problems is still one of the critical issues [61]. Thus, the trial and error process is generally employed to optimize the parameters of GAN models; however, it is a time-consuming and laborious method. A reasonable technique or specific standard for optimizing the parameters of the GAN model is essential. For the next limitation, the 1D CNN model can extract features and diagnose the health state of the composite system, as mentioned above. However, because the 1D CNN model is a black box model, it is unclear which part of the signal was considered, especially for fault diagnosis. To improve this hardship in explainability, the eXplainable Artificial Intelligence (XAI) algorithm will be used in future work. Through the XAI algorithm, it is anticipated that the features that are considered more important in the fault diagnosis process will be identified.

Also, this research focused on evaluating data augmentation performance. For future research, a generalization of the fault diagnosis model will be conducted. For this purpose, a large number of specimens with various conditions will be tested. Then, data augmentation will be implemented for the training dataset to prove that the fault diagnosis model can accurately classify the data that are not trained for the model.

Author Contributions: Conceptualization, S.K., M.M.A., J.S. and H.K.; methodology, S.K., M.M.A. and J.S.; software, S.K.; validation, S.K., M.M.A. and J.S.; formal analysis, S.K. and J.S.; investigation, S.K. and M.M.A.; resources, S.K. and J.S.; data curation, S.K. and M.M.A.; writing—original draft preparation, S.K. and M.M.A.; writing—review and editing, J.S. and H.K.; visualization, S.K.; supervision, J.S. and H.K.; project administration, H.K.; funding acquisition, H.K. All authors have read and agreed to the published version of the manuscript.

Funding: This research was funded by a National Research Foundation of Korea (NRF) grant funded by the Korean government (MSIT) (No. 2020R1A2C1006613) and also supported by the MOTIE (Ministry of Trade, Industry, and Energy) in Korea, under the Fostering Global Talents for Innovative Growth Program (P0017307) supervised by the Korea Institute for Advancement of Technology (KIAT).

Institutional Review Board Statement: Not applicable.

Informed Consent Statement: Not applicable.

Data Availability Statement: Not applicable.

Conflicts of Interest: The authors declare no conflict of interest.

References

1. Zhang, J.; Lin, G.; Vaidya, U.; Wang, H. Past, Present and Future Prospective of Global Carbon Fibre Composite Developments and Applications. *Compos. Part B Eng.* **2023**, *250*, 110463. [\[CrossRef\]](#)
2. Azad, M.M.; Ejaz, M.; Shah, A.R.; Kamran Afaq, S.; Song, J. Static Mechanical Properties of Bio-Fiber-Based Polymer Composites. In *Advances in Bio-Based Fiber*; Elsevier: Amsterdam, The Netherlands, 2022; pp. 97–139.
3. Bui, T.Q.; Hu, X. A Review of Phase-Field Models, Fundamentals and Their Applications to Composite Laminates. *Eng. Fract. Mech.* **2021**, *248*, 107705. [\[CrossRef\]](#)
4. Khalid, S.; Kim, H.S. Recent Studies on Stress Function-Based Approaches for the Free Edge Stress Analysis of Smart Composite Laminates: A Brief Review. *Multiscale Sci. Eng.* **2022**, *4*, 73–78. [\[CrossRef\]](#)
5. Banks-Sills, L. Interface Fracture and Delaminations in Composite Materials; SpringerBriefs. In *Applied Sciences and Technology*; Springer International Publishing: Cham, Switzerland, 2018; ISBN 978-3-319-60326-1.
6. Mortell, D.J.; Tanner, D.A.; McCarthy, C.T. In-Situ SEM Study of Transverse Cracking and Delamination in Laminated Composite Materials. *Compos. Sci. Technol.* **2014**, *105*, 118–126. [\[CrossRef\]](#)
7. Azad, M.M.; Kim, S.; Cheon, Y.B.; Kim, H.S. Intelligent Structural Health Monitoring of Composite Structures Using Machine Learning, Deep Learning, and Transfer Learning: A Review. *Adv. Compos. Mater.* **2023**, 1–27. [\[CrossRef\]](#)
8. Liu, G.; Li, L.; Zhang, L.; Li, Q.; Law, S.S. Sensor Faults Classification for SHM Systems Using Deep Learning-Based Method with Tsfresh Features. *Smart Mater. Struct.* **2020**, *29*, 075005. [\[CrossRef\]](#)
9. Deng, F.; Tao, X.; Wei, P.; Wei, S. A Robust Deep Learning-Based Damage Identification Approach for SHM Considering Missing Data. *Appl. Sci.* **2023**, *13*, 5421. [\[CrossRef\]](#)
10. Finotti, R.P.; Cury, A.A.; Barbosa, F.D.S. An SHM Approach Using Machine Learning and Statistical Indicators Extracted from Raw Dynamic Measurements. *Lat. Am. J. Solids Struct.* **2019**, *16*, e165. [\[CrossRef\]](#)
11. Song, G.; Wang, C.; Wang, B. Structural Health Monitoring (SHM) of Civil Structures. *Appl. Sci.* **2017**, *7*, 789. [\[CrossRef\]](#)
12. Galan-Urbe, E.; Morales-Velazquez, L.; Osornio-Rios, R.A. FPGA-Based Methodology for Detecting Positional Accuracy Degradation in Industrial Robots. *Appl. Sci.* **2023**, *13*, 8493. [\[CrossRef\]](#)
13. Zhang, C.; Mousavi, A.A.; Masri, S.F.; Gholipour, G.; Yan, K.; Li, X. Vibration Feature Extraction Using Signal Processing Techniques for Structural Health Monitoring: A Review. *Mech. Syst. Signal Process.* **2022**, *177*, 109175. [\[CrossRef\]](#)
14. Sohn, H.; Farrar, C.R. Damage Diagnosis Using Time Series Analysis of Vibration Signals. *Smart Mater. Struct.* **2001**, *10*, 446–451. [\[CrossRef\]](#)
15. Tcherniak, D.; Mølgaard, L.L. Vibration-Based SHM System: Application to Wind Turbine Blades. *J. Phys. Conf. Ser.* **2015**, *628*, 012072. [\[CrossRef\]](#)
16. Amezcua-Sanchez, J.P.; Adeli, H. Signal Processing Techniques for Vibration-Based Health Monitoring of Smart Structures. *Arch. Comput. Methods Eng.* **2016**, *23*, 1–15. [\[CrossRef\]](#)
17. Lei, Y.; Yang, B.; Jiang, X.; Jia, F.; Li, N.; Nandi, A.K. Applications of Machine Learning to Machine Fault Diagnosis: A Review and Roadmap. *Mech. Syst. Signal Process.* **2020**, *138*, 106587. [\[CrossRef\]](#)
18. Hoang, D.-T.; Kang, H.-J. A Survey on Deep Learning Based Bearing Fault Diagnosis. *Neurocomputing* **2019**, *335*, 327–335. [\[CrossRef\]](#)
19. Jiang, L.; Yin, H.; Li, X.; Tang, S. Fault Diagnosis of Rotating Machinery Based on Multisensor Information Fusion Using SVM and Time-Domain Features. *Shock Vib.* **2014**, *2014*, 418178. [\[CrossRef\]](#)
20. Samanta, B.; Al-Balushi, K.R. Artificial Neural Network Based Fault Diagnostics of Rolling Element Bearings Using Time-Domain Features. *Mech. Syst. Signal Process.* **2003**, *17*, 317–328. [\[CrossRef\]](#)
21. Ye, L.; Ma, X.; Wen, C. Rotating Machinery Fault Diagnosis Method by Combining Time-Frequency Domain Features and CNN Knowledge Transfer. *Sensors* **2021**, *21*, 8168. [\[CrossRef\]](#)
22. Li, C.; Sanchez, V.; Zurita, G.; Cerrada Lozada, M.; Cabrera, D. Rolling Element Bearing Defect Detection Using the Generalized Synchrosqueezing Transform Guided by Time-Frequency Ridge Enhancement. *ISA Trans.* **2016**, *60*, 274–284. [\[CrossRef\]](#)
23. Hemmati, F.; Orfali, W.; Gadala, M.S. Roller Bearing Acoustic Signature Extraction by Wavelet Packet Transform, Applications in Fault Detection and Size Estimation. *Appl. Acoust.* **2016**, *104*, 101–118. [\[CrossRef\]](#)
24. He, D.; Li, R.; Zhu, J. Plastic Bearing Fault Diagnosis Based on a Two-Step Data Mining Approach. *IEEE Trans. Ind. Electron.* **2012**, *60*, 3429–3440. [\[CrossRef\]](#)
25. Saravanan, N.; Kumar Siddabattuni, V.N.S.; Ramachandran, K.I. A Comparative Study on Classification of Features by SVM and PSVM Extracted Using Morlet Wavelet for Fault Diagnosis of Spur Bevel Gear Box. *Expert Syst. Appl.* **2008**, *35*, 1351–1366. [\[CrossRef\]](#)
26. Amarnath, M.; Sugumaran, V.; Kumar, H. Exploiting Sound Signals for Fault Diagnosis of Bearings Using Decision Tree. *Measurement* **2013**, *46*, 1250–1256. [\[CrossRef\]](#)
27. Zhong, S.; Fu, S.; Lin, L. A Novel Gas Turbine Fault Diagnosis Method Based on Transfer Learning with CNN. *Measurement* **2019**, *137*, 435–453. [\[CrossRef\]](#)

28. Janssens, O.; Slavkovikj, V.; Vervisch, B.; Stockman, K.; Loccufier, M.; Verstockt, S.; Van De Walle, R.; Van Hoecke, S. Convolutional Neural Network Based Fault Detection for Rotating Machinery. *J. Sound Vib.* **2016**, *377*, 331–345. [\[CrossRef\]](#)
29. Hsueh, Y.-M.; Ittangihal, V.R.; Wu, W.-B.; Chang, H.-C.; Kuo, C.-C. Fault Diagnosis System for Induction Motors by CNN Using Empirical Wavelet Transform. *Symmetry* **2019**, *11*, 1212. [\[CrossRef\]](#)
30. Khan, A.; Ko, D.-K.; Lim, S.C.; Kim, H.S. Structural Vibration-Based Classification and Prediction of Delamination in Smart Composite Laminates Using Deep Learning Neural Network. *Compos. Part B Eng.* **2019**, *161*, 586–594. [\[CrossRef\]](#)
31. Tang, X.; Xu, Z.; Wang, Z. A Novel Fault Diagnosis Method of Rolling Bearing Based on Integrated Vision Transformer Model. *Sensors* **2022**, *22*, 3878. [\[CrossRef\]](#)
32. Wen, L.; Li, X.; Gao, L. A Transfer Convolutional Neural Network for Fault Diagnosis Based on ResNet-50. *Neural. Comput. Appl.* **2020**, *32*, 6111–6124. [\[CrossRef\]](#)
33. Zhao, H.; Sun, S.; Jin, B. Sequential Fault Diagnosis Based on LSTM Neural Network. *IEEE Access* **2018**, *6*, 12929–12939. [\[CrossRef\]](#)
34. Yuan, M.; Wu, Y.; Lin, L. Fault Diagnosis and Remaining Useful Life Estimation of Aero Engine Using LSTM Neural Network. In Proceedings of the 2016 IEEE International Conference on Aircraft Utility Systems (AUS), Beijing, China, 8–14 October 2016; IEEE: Piscataway, NJ, USA, 2016; pp. 135–140.
35. Sabir, R.; Rosato, D.; Hartmann, S.; Guehmann, C. LSTM Based Bearing Fault Diagnosis of Electrical Machines Using Motor Current Signal. In Proceedings of the 2019 18th IEEE International Conference on Machine Learning and Applications (ICMLA), Boca Raton, FL, USA, 16–19 December 2019; IEEE: Piscataway, NJ, USA, 2019; pp. 613–618.
36. Zhang, T.; Fei, Q.; Li, N.; Ma, D. Fault Diagnosis Based on Modified BiLSTM Neural Network. In Proceedings of the 2020 5th International Conference on Intelligent Information Technology, Hanoi, Vietnam, 19–22 February 2020; ACM Association for Computing Machinery: New York, NY, USA, 2020; pp. 21–26. [\[CrossRef\]](#)
37. Zhang, W.; Li, X.; Jia, X.-D.; Ma, H.; Luo, Z.; Li, X. Machinery Fault Diagnosis with Imbalanced Data Using Deep Generative Adversarial Networks. *Measurement* **2020**, *152*, 107377. [\[CrossRef\]](#)
38. Khan, A.; Azad, M.M.; Sohail, M.; Kim, H.S. A Review of Physics-Based Models in Prognostics and Health Management of Laminated Composite Structures. *Int. J. Precis. Eng. Manuf. Green Technol.* **2023**, 1–21. [\[CrossRef\]](#)
39. Jung, K.-C.; Chang, S.-H. Advanced Deep Learning Model-Based Impact Characterization Method for Composite Laminates. *Compos. Sci. Technol.* **2021**, *207*, 108713. [\[CrossRef\]](#)
40. Sikdar, S.; Liu, D.; Kundu, A. Acoustic Emission Data Based Deep Learning Approach for Classification and Detection of Damage-Sources in a Composite Panel. *Compos. Part B Eng.* **2022**, *228*, 109450. [\[CrossRef\]](#)
41. Liao, Y.; Qing, X.; Wang, Y.; Zhang, F. Damage Localization for Composite Structure Using Guided Wave Signals with Gramian Angular Field Image Coding and Convolutional Neural Networks. *Compos. Struct.* **2023**, *312*, 116871. [\[CrossRef\]](#)
42. Feng, B.; Cheng, S.; Deng, K.; Kang, Y. Localization of Low-Velocity Impact in CFRP Plate Using Time-Frequency Features of Guided Wave and Convolutional Neural Network. *Wave Motion* **2023**, *119*, 103127. [\[CrossRef\]](#)
43. Cheng, L.; Tong, Z.; Xie, S.; Kersemans, M. IRT-GAN: A Generative Adversarial Network with a Multi-Headed Fusion Strategy for Automated Defect Detection in Composites Using Infrared Thermography. *Compos. Struct.* **2022**, *290*, 115543. [\[CrossRef\]](#)
44. Meister, S.; Möller, N.; Stüve, J.; Groves, R.M. Synthetic Image Data Augmentation for Fibre Layup Inspection Processes: Techniques to Enhance the Data Set. *J. Intell. Manuf.* **2021**, *32*, 1767–1789. [\[CrossRef\]](#)
45. Cheng, L.; Kersemans, M. Dual-IRT-GAN: A Defect-Aware Deep Adversarial Network to Perform Super-Resolution Tasks in Infrared Thermographic Inspection. *Compos. Part B Eng.* **2022**, *247*, 110309. [\[CrossRef\]](#)
46. He, H.; Bai, Y.; Garcia, E.A.; Li, S. ADASYN: Adaptive Synthetic Sampling Approach for Imbalanced Learning. In Proceedings of the 2008 IEEE International Joint Conference on Neural Networks (IEEE World Congress on Computational Intelligence), Hong Kong, China, 1–6 June 2008; IEEE: Piscataway, NJ, USA, 2008; pp. 1322–1328.
47. Marra, A.L.; Juliani, R.; Garcia, C. Data Augmentation for Vibration Signals Using System Identification Techniques. In Proceedings of the 2021 5th International Conference on System Reliability and Safety (ICSRS), Palermo, Italy, 24–26 November 2021; IEEE: Piscataway, NJ, USA, 2021; pp. 281–285.
48. Khan, A.; Raouf, I.; Noh, Y.R.; Lee, D.; Sohn, J.W.; Kim, H.S. Autonomous Assessment of Delamination in Laminated Composites Using Deep Learning and Data Augmentation. *Compos. Struct.* **2022**, *290*, 115502. [\[CrossRef\]](#)
49. Phan, M.; Solbeck, J.; Ray, L. A Direct Method for State-Space Model and Observer/Kalman Filter Gain Identification. In Proceedings of the AIAA Guidance, Navigation, and Control Conference and Exhibit, American Institute of Aeronautics and Astronautics, Providence, RI, USA, 16–19 August 2004.
50. Yang, Z.; Li, Y.; Zhou, G. TS-GAN: Time-Series GAN for Sensor-Based Health Data Augmentation. *ACM Trans. Comput. Healthc.* **2023**, *4*, 1–21. [\[CrossRef\]](#)
51. Lu, H.; Du, M.; Qian, K.; He, X.; Wang, K. GAN-Based Data Augmentation Strategy for Sensor Anomaly Detection in Industrial Robots. *IEEE Sens. J.* **2022**, *22*, 17464–17474. [\[CrossRef\]](#)
52. Smith, K.E.; Smith, A.O. Conditional GAN for Timeseries Generation. *arXiv* **2020**, arXiv:2006.16477v1.
53. Boicea, V.A.; Ulmeanu, A.P.; Vulpe-Grigorași, A. A Novel Approach for Power Load Forecast Based on GAN Data Augmentation. *IOP Conf. Ser. Mater. Sci. Eng.* **2022**, *1254*, 012030. [\[CrossRef\]](#)
54. Arjovsky, M.; Bottou, L. Towards Principled Methods for Training Generative Adversarial Networks. *arXiv* **2017**, arXiv:1701.04862v1.
55. Goodfellow, I. NIPS 2016 Tutorial: Generative Adversarial Networks. *arXiv* **2017**, arXiv:1701.00160v4.

56. Arjovsky, M.; Chintala, S.; Bottou, L. Wasserstein GAN. *arXiv* **2017**, arXiv:1701.07875v3.
57. Tang, S.; Yuan, S.; Zhu, Y. Data Preprocessing Techniques in Convolutional Neural Network Based on Fault Diagnosis towards Rotating Machinery. *IEEE Access* **2020**, *8*, 149487–149496. [[CrossRef](#)]
58. Neupane, D.; Kim, Y.; Seok, J.; Hong, J. CNN-Based Fault Detection for Smart Manufacturing. *Appl. Sci.* **2021**, *11*, 11732. [[CrossRef](#)]
59. Chen, C.-C.; Liu, Z.; Yang, G.; Wu, C.-C.; Ye, Q. An Improved Fault Diagnosis Using 1D-Convolutional Neural Network Model. *Electronics* **2020**, *10*, 59. [[CrossRef](#)]
60. Fu, Q.; Wang, H. A Novel Deep Learning System with Data Augmentation for Machine Fault Diagnosis from Vibration Signals. *Appl. Sci.* **2020**, *10*, 5765. [[CrossRef](#)]
61. Thanh-Tung, H.; Tran, T.; Venkatesh, S. Improving Generalization and Stability of Generative Adversarial Networks. *arXiv* **2019**, arXiv:1902.03984v1.

Disclaimer/Publisher’s Note: The statements, opinions and data contained in all publications are solely those of the individual author(s) and contributor(s) and not of MDPI and/or the editor(s). MDPI and/or the editor(s) disclaim responsibility for any injury to people or property resulting from any ideas, methods, instructions or products referred to in the content.